Geophysical Research Letters

RESEARCH LETTER
10.1029/2024GL110551

Key Points:

- Transient responses of tropical Pacific are sensitive to the hemisphere in which the extratropical radiative forcing is imposed
- Initially, the northern extratropical forcing is more effective at inducing Walker Cell changes
- On longer timescales, the southern extratropical heating exerts larger sea surface temperature increase in the equatorial Pacific

Supporting Information:

Supporting Information may be found in the online version of this article.

Correspondence to:

Y.-T. Hwang,
ythwang@ntu.edu.tw

Citation:

Tseng, H.-Y., & Hwang, Y.-T. (2024). Contrasting the evolution of the tropical Pacific SST responses to time-invariant extratropical forcings in the two hemispheres. *Geophysical Research Letters*, *51*, e2024GL110551. https://doi.org/10.1029/2024GL110551

Received 31 MAY 2024
Accepted 31 OCT 2024

Author Contributions:

Conceptualization: Yen-Ting Hwang
Formal analysis: Hung-Yi Tseng
Funding acquisition: Yen-Ting Hwang
Investigation: Hung-Yi Tseng
Supervision: Yen-Ting Hwang
Validation: Yen-Ting Hwang
Visualization: Hung-Yi Tseng
Writing – original draft: Hung-Yi Tseng
Writing – review & editing: Yen-Ting Hwang

Contrasting the Evolution of the Tropical Pacific SST Responses to Time-Invariant Extratropical Forcings in the Two Hemispheres

Hung-Yi Tseng[1] **and Yen-Ting Hwang**[1]

[1]Department of Atmospheric Sciences, National Taiwan University, Taipei, Taiwan

Abstract We compare the equatorial Pacific sea surface temperature (SST) responses to radiative forcings in the extratropics of each hemispehre, with heating or cooling imposed in either hemisphere using a fully coupled climate model. In the initial 3 years, the equatorial SST responses exhibit an opposite sign to the forcings in the northern extratropics but align with those in the southern extratropics. At this stage, heating the northern extratropics is more effective at cooling the equatorial Pacific than cooling the southern extratropics. This occurs because the anomalous warming in the northern extratropics is blocked by the rainband and can only enter the equatorial Pacific from the west, triggering Bjerknes feedback more effectively. Over a decade, all experiments show enhanced equatorial responses aligning with the signs of the forcings. The south-perturbed cases experience stronger equatorial SST responses, suggesting the significant control of the southern extratropics on tropical Pacific on decadal timescales.

Plain Language Summary The center of the Hadley circulation is north of the equator and the oceanic subtropical cell in the Southern Hemisphere is stronger than that in the north. These cause an uneven response in equatorial Pacific sea surface temperatures (SST) to forcings from the Northern and the Southern Hemispheres. We use a set of idealized experiments to compare the tropical Pacific responses to radiative forcings from the extratropics of the two hemispheres. Our findings show that the northern extratropical region has a stronger impact on the equatorial Pacific via a teleconnection pathway influenced by air-sea fluxes. The northward-displaced climatological rainband blocks the anomalous SST from the northern extratropics and forces the anomalies entering the tropical Pacific region from the west. This reinforces the meridional gradient in the eastern Pacific and the zonal gradient over the equatorial central Pacific, leading to stronger atmospheric circulation and SST responses. In contrast, the southern extratropics is efficiently connected to the equatorial Pacific region via the oceanic circulation for the delayed responses. The mechanisms discussed in our study are relevant for interpreting the cooling trend in the equatorial Pacific in recent decades and for predicting the increasingly important control from the Southern Ocean.

1. Introduction

Sea surface temperature (SST) variations in the tropical Pacific region profoundly impact regional and global climate. They regulate local deep convections and thus influence teleconnections to the extratropics via stationary Rossby waves (Trenberth et al., 1998), which strongly affect extreme weather events (W. Anderson et al., 2023; Seager et al., 2015; Sobel et al., 2023). Moreover, the temporal and spatial evolutions of SST in the tropical Pacific region can alter the rate of global warming, as they strongly influence the vertical structures of atmospheric temperature and subsequent radiative effects, referred to as the "pattern effect" (Andrews et al., 2015; Ceppi & Gregory, 2017; Dong et al., 2019; Rugenstein et al., 2023).

Many recent literature discuss the responses of tropical Pacific SST to rising greenhouse gases. Through performing global climate model (GCM) experiments with abrupt $4 \times CO_2$ and 1% CO_2 experiments in the Coupled Model Intercomparison Project (CMIP) Phase 5/6 (Heede et al., 2020, 2021; Heede & Fedorov, 2021; Long & Collins, 2013; Luo et al., 2018) and an abrupt return of CO_2 levels to preindustrial conditions (Held et al., 2010), mechanisms with multiple timescales are identified. The dynamical thermostat mechanism, triggered by the delayed warming over the climatological upwelling region (Clement et al., 1996), explains the short-term cooling of the equatorial Pacific SST and may contribute to part of the observed trend (Heede et al., 2021; Heede & Fedorov, 2023; Seager et al., 2019). On a longer timescale, an eastern equatorial-enhanced SST warming is expected. This warming can be attributed to several mechanisms, including the atmospheric or surface energetic

constraint that predicts a weakening of the Walker cell (Held & Soden, 2006; Vecchi & Soden, 2007; Xie et al., 2010) and the anomalously warmed equatorial upwelling due to the advection of extratropical warm SST anomalies via the subtropical cells (Heede et al., 2020; Li et al., 2024).

In addition to the well-mixed greenhouse gases, extratropical energy perturbations also have the potential to affect tropical Pacific SST. For example, the emissions of anthropogenic aerosols that are primarily concentrated in the Northern Hemisphere (NH) industrial regions (Hwang et al., 2024; Takahashi & Watanabe, 2016; Wang et al., 2019), the Antarctica ozone hole (Hartmann, 2022), the missing freshwater forcing from ice sheet melting in global climate models (Bintanja et al., 2013; Bronselaer et al., 2018; Dong, Pauling, et al., 2022; Pauling et al., 2016; Sadai et al., 2020), and the recent cooling trend over the Southern Ocean that global climate models failed to capture have all been proposed to alter tropical Pacific SST in observed records or climate model simulations.

The aforementioned forcings originate from both the Northern and the Southern mid-to-high latitude regions, and their respective contributions to the tropical Pacific SST response patterns require further exploration. Modeling studies using idealized slab ocean settings often highlight a strong linkage between the Southern Ocean and the eastern tropical Pacific (Hwang et al., 2017; Kang et al., 2020). A two-way teleconnection through atmospheric circulations indicates the strong and effective control by extratropical region in the Southern Hemisphere (SH) on the tropical Pacific SST, suggesting the decreased SST in the southeast Pacific Ocean sector influences the equatorial Pacific cooling trend in the 45-year observational data (Dong, Armour, et al., 2022). On the other hand, in fully coupled models, the equatorial SST exhibits similar responses to ice melting or idealized insolation changes in both hemispheres (M. R. England et al., 2020; Kang et al., 2020). Challenges arise when linking the mechanistic understanding of equilibrium responses to more realistic situations. For instance, simulations with the observed Southern Ocean cooling trend exhibit much weaker equatorial Pacific SST responses than expected based on equilibrium responses (Kang, Yu, et al., 2023; Xiyue Zhang et al., 2021). Likewise, freshwater hosing experiments require unrealistically strong forcings to produce robust tropical responses (Dong, Pauling, et al., 2022; Pauling et al., 2016).

The relative importance of northern and southern extratropical influences on the tropical Pacific needs to be understood within a framework that considers multiple timescales. To reach the goal, this study uses a fully coupled GCM and performs two sets of experiments, each applying an instantaneous radiative forcing of identical magnitude in the extratropical regions of either hemisphere. The energy perturbation introduced into the system can represent various types of radiative forcings concentrated in the extratropics, including those induced by anthropogenic aerosols, volcano eruptions, or radiative feedbacks associated with global warming. Our findings can be applied to interpreting the tropical responses in climate change scenarios.

2. Methods

We employ the National Center for Atmospheric Research (NCAR) Community Earth System Model (CESM) version 1.2.0, where the Community Atmospheric Model Version 5 (CAM5) with 30 vertical levels and a 1.9° latitude by 2.5° longitude horizontal resolution is coupled to the Parallel Ocean Program, Version 2 (POP2), using the "gx1v6" displaced pole grid and has a resolution of ∼1° near the equator (Hurrell et al., 2013). The incoming solar radiation at the top of the atmosphere is increased or reduced between 45°–65° in either the NH or the SH as heating or cooling forcing (Figure S1 in Supporting Information S1), and these insolation perturbations contain seasonal and diurnal cycles. These idealized forcings, originally designed to investigate the impacts of extratropical cloud bias on tropical climate (Kang et al., 2019), have also proven useful in understanding anthropogenic climate change (Kang et al., 2020; Luongo et al., 2023; Tseng et al., 2023). To narrow down the influences of internal variability, we conduct 30 ensembles, branched from 30 consecutive January conditions from a 180-year control simulation under pre-industrial forcing. These ensembles are integrated for five years, and 20 are extended to 20 years to examine long-term responses.

In this paper, we only discuss the linear component, defined by subtracting the responses to cooling from the responses to heating and dividing by two. Thus, the figures shown in this study are similar to the results of the heating cases and can be qualitatively viewed as the cooling case responses with their signs reversed. The SST responses of the individual experiments can be found in the Supplementary (Figures S2 and S3 in Supporting Information S1). In the main text, we refer to the two experiments with forcings imposed in the northern (southern) extratropics as NH (SH) Case and only demonstrate the linear components for simplicity. We neglect

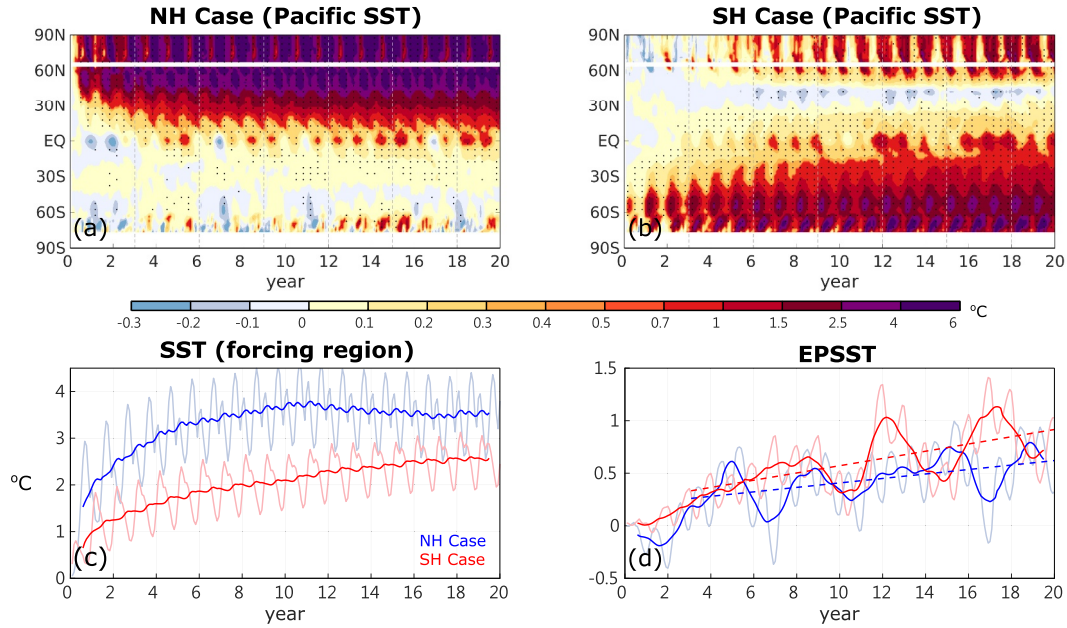

Figure 1. SST evolution. The temporal evolutions of zonal averaged SST anomalies in the Pacific region (160°E–90°W) in (a) NH Case and (b) SH Case, the temporal evolutions of the SST anomalies averaged in (c) forcing region (45°N–65°N for NH Case, and 45°S–65°S for SH Case) and (d) equatorial Pacific region (160°E–90°W, 5°N–5°S). Stippling in (a) and (b) indicates the statistically significant responses at a 95% confidence interval. In (c) and (d), the thin lines represent the monthly anomalies, whereas thick lines are the 1-year running mean. The dashed lines in (d) are the linear trends of the equatorial SST during years 3–20 of the two cases.

the nonlinear terms, which can be quantified by averaging the responses from the heating and cooling cases. They are small, particularly in the tropical Pacific region (Figure S4 in Supporting Information S1).

The forcings are applied as a step-function, meaning they are abruptly introduced at the start and maintained throughout the simulations. By examining the transient evolution of tropical responses under these perpetual forcing conditions, we can effectively distinguish between the immediate (fast) and gradual (slow) responses of the system. A similar step-function approach was used for decomposing the system's responses to greenhouse gases (Good et al., 2011, 2013; Heede et al., 2020, 2021; Held et al., 2010; Long & Collins, 2013) and aerosol forcings (Hwang et al., 2024) across multiple timescales.

3. Local and Remote SST Responses

We first discuss the evolutions of the zonal mean SST responses in the two sets of experiments. In the forcing region, the SST response in NH Case is stronger than that in SH Case (Figures 1a and 1b), which can be understood by the deeper mixed layer depth and the climatological upwelling in the Southern Ocean. The SST responses in both experiments peak in the summer months, reflecting the seasonal variation of the imposed forcings (Figure 1c).

Despite the pronounced local SST warming in the northern extratropics, NH Case experiences significant cooling in the equatorial Pacific region during the initial 3 years, and the gradual warming expected from imposing heating does not occur until the fourth year (Figures 1a and 1d). SH Case, on the other hand, shows a relatively weak equatorial SST response at the beginning of the simulations (Figure 1b), but a stronger warming trend (Figure 1d). Furthermore, the seasonalities of the equatorial SST responses in both cases are distinct from those in the forcing regions—the equatorial SST warming reaches its maximum in December in SH Case, while during the same period the equator experiences less warming in NH Case (Figure 1d). This may be attributed to the stronger joint cloud wind-evaporation-SST feedback (joint cloud-WES feedback) in the southeast Pacific during austral summer (You & Furtado, 2018; H. Zhang, Clement, & Di Nezio, 2014), which tends to cool the equator in NH Case while warm the equator in SH Case.

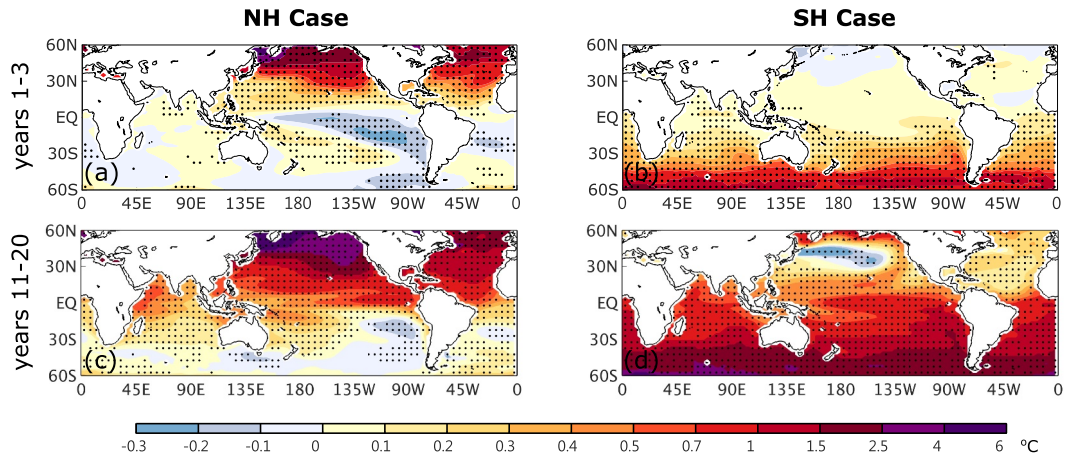

Figure 2. SST response. SST anomalies in (a) NH Case and (b) SH Case, during the initial 3 years. (c, d) are the same as (a, b), but for years 11–20. Stippling indicates the statistically significant responses at a 95% confidence interval.

In the following, we investigate the air-sea flux and ocean dynamic mechanisms that shape the tropical Pacific SST response patterns. Both mechanisms contribute to rapid equatorial warming in decadal timescales when the SH extratropic is heated.

4. Thermodynamic Air-Sea Fluxes and the Contrasting Initial Equatorial SST Responses

During the initial 3 years, the anomalous equatorial SSTs in both cases appear to be correlated with the SST anomalies in the southeastern Pacific region (Figures 2a and 2b). Specifically, NH Case displays a more pronounced cooling trend, particularly in the central equatorial region, whereas a weak SST warming is exhibited in the eastern equatorial region in SH Case.

The spatial patterns can be attributed to air-sea interactions associated with the anomalous cross-equatorial Hadley circulation, supported by the short response timescale and the anomalous temperature peaking at the surface (Figures S5a and S5b in Supporting Information S1). In NH Case, responding to the imposed radiative perturbation, an anomalous cross-equatorial atmospheric circulation is established, transporting excessive energy from the Northern to the Southern Hemisphere through its upper branch (Figure S6a in Supporting Information S1). Its lower branch features anomalous cross-equatorial southerly winds (Figure S6c in Supporting Information S1), strengthening the climatological trades in the southeastern Pacific region, cooling local SSTs and propagating them toward the equator via the joint cloud-WES feedback (Hsiao et al., 2022; Kang et al., 2020; H. Zhang, Clement, & Di Nezio, 2014). In SH Case, the anomalous cross-equatorial Hadley Cell exhibits the opposite direction (Figure S6b in Supporting Information S1). The anomalous northerlies across the equator weaken the climatological trades and result in anomalous warming (Figure 2b). The differing responses in the two cases can be attributed to the northward displacement of the climatological intertropical convergence zone (ITCZ). The SST responses in the southern subtropics in the two cases can penetrate the equatorial region, whereas signals from the north are blocked by the ITCZ (Figures 3a, 3b, 3c and S7, Kang et al., 2020; Tseng et al., 2023). Furthermore, the contrasting cross-equatorial wind changes in the eastern equatorial Pacific region lead to distinct thermocline responses by altering the strength of oceanic mixing and upwelling (Hu & Fedorov, 2018), which are consistent with the equatorial SST responses in the two cases (compare Figure S5a to Figure and Figure S5b in Supporting Information S1).

During the initial 3 years, the cold tongue region SST, the Indo-Pacific zonal SST gradient, and the indicating Walker circulation responses in NH Case are much more significant than those in SH Case (Figures 2a, 2b, 3d, and 3e). We offer three explanations for the stronger Walker Cell response in NH: (a) The SST responses in the forced region, and thus the associated atmospheric circulation adjustments and air-sea interactions, are weaker in SH Case (see also Figures 1a–1c). However, when normalized by the forcing region SST, the contrast still holds,

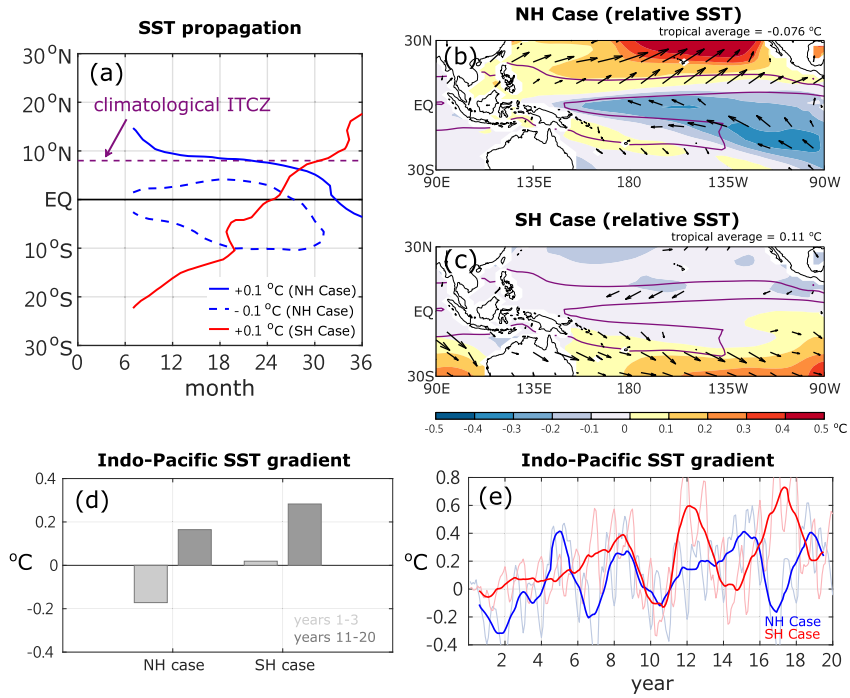

Figure 3. Tropical SST evolution during initial 3 years. (a) The temporal evolutions of latitude where the 1-year running mean Pacific SST anomalies (averaged in 160°E–90°W) are ± 0.1°C (NH Case, blue) and 0.1°C (SH Case, red). Anomalous SST relative to tropical Pacific average (160°E–90°W and 30°S–30°N; shading), the climatological precipitation (purple contours, CI = 3,000 mm/year) and anomalous surface wind stress (vector) during years 1–3 in (b) NH Case and (c) SH Case. (d) The equatorial (5°N–5°S) SST gradient (°C, difference between 160°W–80°W and 80°E–180°, following Heede et al., 2020) averaged (°C) in years 1–3 (light gray) and years 11–20 (dark gray), and (e) the temporal evolutions of monthly (thin) and 1-year running mean (thick) zonal equatorial SST gradient anomalies in the two cases. In (a), the purple dashed line indicates the latitude of the climatological ITCZ. Only wind stress responses that are statistically significant are shown in (b) and (c).

indicating further factors leading to the difference (not shown). (b) In NH Case, the anomalously warmed SST in the northern extratropics is blocked by the climatological intertropical convergence zone (ITCZ) when propagates toward the warm pool. The joint WES-cloud feedback brings the anomalous warming toward the warm pool, sharpening the equatorial zonal contrast and enhancing the equatorial coupled dynamics. The resulted anomalous easterly amplifies anomalous cooling over the cold tongue, further enhancing both the equatorial zonal SST gradient and the meridional SST gradient across the equator (Figure 3b) (B. T. Anderson et al., 2013; M. H. England et al., 2014; Latif et al., 2023; Tseng et al., 2023). (c) The tropical Indian and Atlantic Oceans experience significant warming in the initial years in SH Case (Figure 2b), potentially dampening the warming in the equatorial Pacific through inter-basin processes (Ferster et al., 2023; Kucharski et al., 2011; Kucharski et al., 2015; Luo et al., 2012; Rodríguez-Fonseca et al., 2009; L. Zhang et al., 2019).

5. Dynamical Oceanic Processes Explaining the Emerging Equatorial Warming in Both Cases

After one decade, both cases experience eastern equatorial-enhanced warming (Figures 2c and 2d). In NH Case, this warming is disconnected from the equatorward propagating signal originating in the forced region, which affects the western equatorial region (compare Figure 2a and Figure S5a in Supporting Information S1 with Figure 2c and Figure S5c in Supporting Information S1). On the contrary, the warming in SH Case appears to be partly linked to the equatorward-propagating signal from the extratropics, indicated by the smoothly connected spatial pattern (compare Figures 2b and Figure S5b in Supporting Information S1 with Figure 2d and Figure S5d in Supporting Information S1). A closer comparison indicates the SH Case shows a more pronounced equatorial warming than NH Case after the first decade of imposing forcing (Figure 1d).

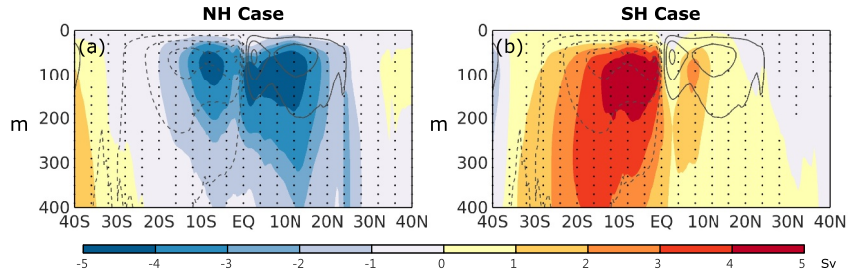

Figure 4. Oceanic Pacific Subtropical cell response. Climatological Pacific meridional overturning circulation (contoured with CI = 10 Sv, zero contour omitted and negative dashed) and the anomalies (shaded) in years 11–20 in (a) NH case and (b) SH case. Stippling indicates the statistically significant responses at a 95% confidence interval.

This SST warming pattern can be attributed to oceanic dynamical processes. The linkage between the imposed interhemispheric energy imbalance and the oceanic circulation responses has been understood via two perspectives: (a) The wind-driven component, where the anomalous cross-equatorial Hadley circulation (Figures S8a and S8b in Supporting Information S1) and the accompanying anomalous surface wind stress (Figures S8c and S8d in Supporting Information S1) trigger the cross-equatorial oceanic circulation response (Green et al., 2019; Green & Marshall, 2017). (b) The buoyancy-driven component, where the dominance of the buoyancy-forced response in the cross-equatorial oceanic cell in the subtropics is revealed in wind stress overriding experiments (Luongo et al., 2022, 2023). Both perspectives indicate the robust weakening of the oceanic subtropical cells (STCs), specifically in the forced hemisphere (Figure 4). The slowdown of the STC thus converges excessive heat on the equator, leading to the equatorial warming (Figure S9 in Supporting Information S1). Moreover, as the Equatorial Undercurrent (EUC) is tightly linked to the southern STC (Kuntz & Schrag, 2018; Liu et al., 1994), the accompanying slowdown of the EUC also contributes to the warming on the equator in SH Case (Figure S9b in Supporting Information S1).

The equatorial warming trend (Figure 1d), the equatorial zonal SST gradient and, the Walker circulation responses (Figures 3d and 3e) are larger in SH Case. There could be three explanations: (a) The weakening response of the STC in the forced hemisphere is more pronounced and penetrates deeper in SH Case, resulting in a more significant weakening of poleward energy transport. (b) In SH Case, the weakening trades in the Southeastern Pacific and the equatorial regions persist in the second decade (Figure S8d in Supporting Information S1). The resultant equatorial SST warming anomalies tend to amplify the aforementioned oceanic circulation-induced SST response on the equator. On the contrary, the strengthening trades and the associated air-sea fluxes in the southeastern Pacific in turn compensate for the oceanic circulation-induced warming in NH Case (Figure S8c in Supporting Information S1). (c) Given that most of the continents are in the NH, the absorption of the imposed radiative heating by the ocean is larger in SH Case (Figure S10 in Supporting Information S1), while a portion of the imposed radiative forcing over the continents is offset by increased outgoing longwave radiation locally, resulting in a smaller change in oceanic energy transport and weaker remote effects in NH Case. In sum, the energy entering the ocean, the initial fast response, and the subsequent slow oceanic adjustments all contribute to a stronger equatorial warming in SH Case compared to NH case during the second decade.

6. Summary and Discussion

This study compares the evolutions of the tropical Pacific SST patterns in response to perturbed insolation in the northern and southern extratropics. Distinct evolutions are observed: (a) During the initial 3 years, heating the southern extratropics results in slight warming in the eastern equatorial region, whereas heating the northern extratropics induces pronounced cooling in the central equatorial region (Figures 2a and 2b). The relatively strong cooling in NH Case can be attributed to the interhemispheric asymmetric pattern driven by an anomalous cross-equatorial Hadley Cell. In the southeast Pacific, strengthened trades initiate the joint cloud-WES feedback, bringing anomalous cooling to the equatorial central Pacific. In the northern tropical Pacific, the northward-displaced climatological ITCZ prevents the warm SST anomalies from reaching the central and eastern equatorial regions. Instead, they propagate westward and southward, reaching the western Pacific and warming the SST in the warm pool region (Figures 2a, 3a, and 3b; Figure S5 in Supporting Information S1). The warming from

the north, the cooling from the south, and the thermocline tilt induced by intensified cross-equatorial trades collectively strengthen the equatorial zonal SST gradient, triggering equatorial air-sea interactions and resulting in stronger equatorial responses (Figures 3d and 3e). (b) After one decade, both cases exhibit eastern equatorial-enhanced warming (Figures 2c and 2d), attributable to the slowdown of the STC in the forced hemisphere, the EUC, and equatorial upwelling. The shallower and weaker STC responses, accompanied by equatorial cooling during the initial 3 years, give rise to the slower and weaker warming over the cold tongue region in NH Case on a decadal timescale (Figure 3e).

While the fast response can only be seen in the first 3 years in our idealized experiments, it may be relevant for long-term climate change. Recent research investigating the fast and slow responses of equatorial Pacific to CO_2 forcing suggests that the strengthened Walker Cell lasting for only 20 years in the step-function $4 \times CO_2$ experiment may last up to 100 years in the experiments with gradual CO_2 increase (Heede et al., 2020). Likewise, it is shown that the rapid initial effects of anthropogenic aerosols in idealized constant forcing experiments evolve into long-term linear trends lasting several decades in CMIP simulations using realistic aerosol emission trajectories (Hwang et al., 2024). In a climate change scenario with time-varying extratropical radiative forcings or feedbacks, the fast response reported in this study may superimpose the slow response and contribute to long-term trends.

There are examples of how our understanding of the fast response may help interpret tropical SST responses in more realistic experiments. Consistent with our findings, where the equatorial Pacific is sensitive to northern extratropical forcings in inter-annual timescales, volcano eruptions in the NH have been reported to be more likely to trigger El Niño events than those in the SH (Erez & Adam, 2021; Pausata et al., 2020). Furthermore, Hwang et al. (2024) use the same mechanisms operating in our NH Case to explain why the aerosol-induced equatorial cooling peaks when aerosol loading starts to decline in climate model simulations. The SST pattern in the initial three years in NH Case (Figure 2a) remarkably resembles the observed SST trends in 1979–2022 (Lee et al., 2022; Wills et al., 2022), suggesting a potential influence of rapid NH warming on cooling the SST in equatorial and southeast Pacific. Our result further implies that heating imposed in the northern extratropics is more efficient in cooling the equatorial region and strengthening the stronger Walker circulation than cooling imposed in the southern extratropics (Figures 2a, 2b, 3d, and 3e). In addition, the SST pattern in the initial 3 years in SH Case (Figure 2b) also resembles those in the Southern Ocean pacemaker experiments (Kang, Ceppi, et al., 2023; Kang, Yu, et al., 2023; Xiyue Zhang et al., 2021), with anomalies penetrating deeper into the equatorial region in the Indian Ocean, insignificant SST changes in the equatorial Pacific region, and pronounced responses in the tropical southeast Pacific.

On longer timescales, our results indicate a strong control of the southern extratropics on the tropical Pacific region. As the Southern Ocean undergoes accelerated warming in future projections, we expect a climate response similar to the slow response demonstrated in our SH Case, exhibiting enhanced equatorial and southeast Pacific warming and significant Walker Cell weakening.

The results and discussions remain to be tested in other GCMs and more realistic climate change scenarios. The hemispheric contrasts revealed in this study may be even more significant in models with smaller mean state biases. Most up-to-date GCMs, including the 2-degree resolution CESM we use, suffer from the double-ITCZ bias, where the rainband remains south of the equator too long throughout the seasonal cycle (Adam et al., 2018; Mechoso et al., 1995; Tian & Dong, 2020; Xiaoxiao Zhang et al., 2015), leading to a less effective ITCZ-blocking effect (H. Zhang, Deser, et al., 2014). Meanwhile, this tends to prevent the SST anomalies in the southeastern Pacific region from propagating equatorward via the joint cloud-WES feedback mechanism. Therefore, our simulations may tend to underestimate the rapid strengthening of the zonal SST gradient and the Walker cell shaping by the air-sea fluxes in the initial responses. Likewise, removing the biased ITCZ and the associated PV barrier in the southern tropical Pacific region reinforces the connection between the Southern extratropics and the equatorial region via the southern STC (Alexander et al., 2006; Capotondi, 2008). The long-term controls of the SH in tropical climates indicated by the slow response could be even more prominent.

Data Availability Statement

Processed data to support the analysis of our CESM simulations and figure codes are publicly available in Tseng (2024).

Acknowledgments
The authors were supported by the National Science and Technology Council of Taiwan (MOST 110-2628-M-002-002, NSTC 111-2628-M-002-003-, and NSTC 112-2111-M-002-016-MY4). Without implying their endorsement, we thank Drs. Sarah Kang, Clara Deser, Shang-Ping Xie, and Yu-Heng Tseng for helpful discussions and suggestions. We acknowledge National Center for High-performance Computing (NCHC) for providing computational and storage resources for the CESM simulations.

References

Adam, O., Schneider, T., & Brient, F. (2018). Regional and seasonal variations of the double-ITCZ bias in CMIP5 models. *Climate Dynamics*, *51*(1), 101–117. https://doi.org/10.1007/s00382-017-3909-1

Alexander, M., Yin, J., Branstator, G., Capotondi, A., Cassou, C., Cullather, R., et al. (2006). Extratropical atmosphere–ocean variability in CCSM3. *Journal of Climate*, *19*(11), 2496–2525. https://doi.org/10.1175/jcli3743.1

Anderson, B. T., Perez, R. C., & Karspeck, A. (2013). Triggering of El Niño onset through trade wind–induced charging of the equatorial Pacific. *Geophysical Research Letters*, *40*(6), 1212–1216. https://doi.org/10.1002/grl.50200

Anderson, W., Cook, B. I., Slinski, K., Schwarzwald, K., McNally, A., & Funk, C. (2023). Multiyear La Niña events and multiseason drought in the Horn of Africa. *Journal of Hydrometeorology*, *24*(1), 119–131. https://doi.org/10.1175/jhm-d-22-0043.1

Andrews, T., Gregory, J. M., & Webb, M. J. (2015). The dependence of radiative forcing and feedback on evolving patterns of surface temperature change in climate models. *Journal of Climate*, *28*(4), 1630–1648. https://doi.org/10.1175/jcli-d-14-00545.1

Bintanja, R., van Oldenborgh, G. J., Drijfhout, S. S., Wouters, B., & Katsman, C. A. (2013). Important role for ocean warming and increased ice-shelf melt in Antarctic sea-ice expansion. *Nature Geoscience*, *6*(5), 376–379. https://doi.org/10.1038/ngeo1767

Bronselaer, B., Winton, M., Griffies, S. M., Hurlin, W. J., Rodgers, K. B., Sergienko, O. V., et al. (2018). Change in future climate due to Antarctic meltwater. *Nature*, *564*(7734), 53–58. https://doi.org/10.1038/s41586-018-0712-z

Capotondi, A. (2008). Can the mean structure of the tropical pycnocline affect ENSO period in coupled climate models? *Ocean Modelling*, *20*(2), 157–169. https://doi.org/10.1016/j.ocemod.2007.08.003

Ceppi, P., & Gregory, J. M. (2017). Relationship of tropospheric stability to climate sensitivity and Earth's observed radiation budget. *Proceedings of the National Academy of Sciences*, *114*(50), 13126–13131. https://doi.org/10.1073/pnas.1714308114

Clement, A. C., Seager, R., Cane, M. A., & Zebiak, S. E. (1996). An Ocean dynamical thermostat. *Journal of Climate*, *9*(9), 2190–2196. https://doi.org/10.1175/1520-0442(1996)009<2190:aodt>2.0.co;2

Dong, Y., Armour, K. C., Battisti, D. S., & Blanchard-Wrigglesworth, E. (2022). Two-way teleconnections between the Southern Ocean and the tropical pacific via a dynamic feedback. *Journal of Climate*, *35*(19), 6267–6282. https://doi.org/10.1175/jcli-d-22-0080.1

Dong, Y., Pauling, A. G., Sadai, S., & Armour, K. C. (2022). Antarctic ice-sheet meltwater reduces transient warming and climate sensitivity through the sea-surface temperature pattern effect. *Geophysical Research Letters*, *49*(24), e2022GL101249. https://doi.org/10.1029/2022GL101249

Dong, Y., Proistosescu, C., Armour, K. C., & Battisti, D. S. (2019). Attributing historical and future evolution of radiative feedbacks to regional warming patterns using a green's function approach: The preeminence of the western pacific. *Journal of Climate*, *32*(17), 5471–5491. https://doi.org/10.1175/jcli-d-18-0843.1

England, M. H., McGregor, S., Spence, P., Meehl, G. A., Timmermann, A., Cai, W., et al. (2014). Recent intensification of wind-driven circulation in the Pacific and the ongoing warming hiatus. *Nature Climate Change*, *4*(3), 222–227. https://doi.org/10.1038/nclimate2106

England, M. R., Polvani, L. M., Sun, L., & Deser, C. (2020). Tropical climate responses to projected Arctic and Antarctic sea-ice loss. *Nature Geoscience*, *13*(4), 275–281. https://doi.org/10.1038/s41561-020-0546-9

Erez, M., & Adam, O. (2021). Energetic constraints on the time-dependent response of the ITCZ to volcanic eruptions. *Journal of Climate*, *34*(24), 9989–10006. https://journals.ametsoc.org/view/journals/clim/34/24/JCLI-D-21-0146.1.xml

Ferster, B. S., Fedorov, A. V., Guilyardi, E., & Mignot, J. (2023). The effect of Indian ocean temperature on the pacific trade winds and ENSO. *Geophysical Research Letters*, *50*(20), e2023GL103230. https://doi.org/10.1029/2023GL103230

Good, P., Gregory, J. M., & Lowe, J. A. (2011). A step-response simple climate model to reconstruct and interpret AOGCM projections. *Geophysical Research Letters*, *38*(1). https://doi.org/10.1029/2010GL045208

Good, P., Gregory, J. M., Lowe, J. A., & Andrews, T. (2013). Abrupt CO2 experiments as tools for predicting and understanding CMIP5 representative concentration pathway projections. *Climate Dynamics*, *40*(3), 1041–1053. https://doi.org/10.1007/s00382-012-1410-4

Green, B., & Marshall, J. (2017). Coupling of trade winds with ocean circulation damps ITCZ shifts. *Journal of Climate*, *30*(12), 4395–4411. https://doi.org/10.1175/jcli-d-16-0818.1

Green, B., Marshall, J., & Campin, J.-M. (2019). The 'sticky' ITCZ: Ocean-moderated ITCZ shifts. *Climate Dynamics*, *53*(1), 1–19. https://doi.org/10.1007/s00382-019-04623-5

Hartmann, D. L. (2022). The Antarctic ozone hole and the pattern effect on climate sensitivity. *Proceedings of the National Academy of Sciences of the U S A*, *119*(35), e2207889119. https://doi.org/10.1073/pnas.2207889119

Heede, U. K., & Fedorov, A. V. (2021). Eastern equatorial Pacific warming delayed by aerosols and thermostat response to CO2 increase. *Nature Climate Change*, *11*(8), 696–703. https://doi.org/10.1038/s41558-021-01101-x

Heede, U. K., & Fedorov, A. V. (2023). Colder eastern equatorial pacific and stronger walker circulation in the early 21st century: Separating the forced response to global warming from natural variability. *Geophysical Research Letters*, *50*(3), e2022GL101020. https://doi.org/10.1029/2022GL101020

Heede, U. K., Fedorov, A. V., & Burls, N. J. (2020). Time scales and mechanisms for the tropical pacific response to global warming: A tug of war between the ocean thermostat and weaker walker. *Journal of Climate*, *33*(14), 6101–6118. https://doi.org/10.1175/jcli-d-19-0690.1

Heede, U. K., Fedorov, A. V., & Burls, N. J. (2021). A stronger versus weaker walker: Understanding model differences in fast and slow tropical pacific responses to global warming. *Climate Dynamics*, *57*(9), 2505–2522. https://doi.org/10.1007/s00382-021-05818-5

Held, I. M., & Soden, B. J. (2006). Robust responses of the hydrological cycle to global warming. *Journal of Climate*, *19*(21), 5686–5699. https://doi.org/10.1175/jcli3990.1

Held, I. M., Winton, M., Takahashi, K., Delworth, T., Zeng, F., & Vallis, G. K. (2010). Probing the fast and slow components of global warming by returning abruptly to preindustrial forcing. *Journal of Climate*, *23*(9), 2418–2427. https://doi.org/10.1175/2009jcli3466.1

Hsiao, W.-T., Hwang, Y.-T., Chen, Y.-J., & Kang, S. M. (2022). The role of clouds in shaping tropical pacific response pattern to extratropical thermal forcing. *Geophysical Research Letters*, *49*(11), e2022GL098023. https://doi.org/10.1029/2022GL098023

Hu, S., & Fedorov, A. V. (2018). Cross-equatorial winds control El Niño diversity and change. *Nature Climate Change*, *8*(9), 798–802. https://doi.org/10.1038/s41558-018-0248-0

Hurrell, J. W., Holland, M. M., Gent, P. R., Ghan, S., Kay, J. E., Kushner, P. J., et al. (2013). The community Earth system model: A framework for collaborative research. *Bulletin of the American Meteorological Society*, *94*(9), 1339–1360. https://doi.org/10.1175/bams-d-12-00121.1

Hwang, Y.-T., Xie, S.-P., Chen, P.-J., Tseng, H.-Y., & Deser, C. (2024). Contribution of anthropogenic aerosols to persistent La Niña-like conditions in the early 21st century. *Proceedings of the National Academy of Sciences*, *121*(5), e2315124121. https://doi.org/10.1073/pnas.2315124121

Hwang, Y.-T., Xie, S.-P., Deser, C., & Kang, S. M. (2017). Connecting tropical climate change with Southern Ocean heat uptake. *Geophysical Research Letters*, *44*(18), 9449–9457. https://doi.org/10.1002/2017GL074972

Kang, S. M., Ceppi, P., Yu, Y., & Kang, I.-S. (2023). Recent global climate feedback controlled by Southern Ocean cooling. *Nature Geoscience*, *16*(9), 775–780. https://doi.org/10.1038/s41561-023-01256-6

Kang, S. M., Hawcroft, M., Xiang, B., Hwang, Y.-T., Cazes, G., Codron, F., et al. (2019). Extratropical–tropical interaction model Intercomparison Project (Etin-Mip): Protocol and initial results. *Bulletin of the American Meteorological Society*, *100*(12), 2589–2606. https://doi.org/10.1175/bams-d-18-0301.1

Kang, S. M., Xie, S.-P., Shin, Y., Kim, H., Hwang, Y.-T., Stuecker, M. F., et al. (2020). Walker circulation response to extratropical radiative forcing. *Science Advances*, *6*(47), eabd3021. https://doi.org/10.1126/sciadv.abd3021

Kang, S. M., Yu, Y., Deser, C., Zhang, X., Kang, I.-S., Lee, S.-S., et al. (2023). Global impacts of recent Southern Ocean cooling. *Proceedings of the National Academy of Sciences*, *120*(30), e2300881120. https://doi.org/10.1073/pnas.2300881120

Kucharski, F., Kang, I.-S., Farneti, R., & Feudale, L. (2011). Tropical Pacific response to 20th century Atlantic warming. *Geophysical Research Letters*, *38*(3). https://doi.org/10.1029/2010GL046248

Kucharski, F., Syed, F. S., Burhan, A., Farah, I., & Gohar, A. (2015). Tropical Atlantic influence on Pacific variability and mean state in the twentieth century in observations and CMIP5. *Climate Dynamics*, *44*(3), 881–896. https://doi.org/10.1007/s00382-014-2228-z

Kuntz, L. B., & Schrag, D. P. (2018). Hemispheric asymmetry in the ventilated thermocline of the tropical pacific. *Journal of Climate*, *31*(3), 1281–1288. https://doi.org/10.1175/jcli-d-17-0686.1

Latif, M., Bayr, T., Kjellsson, J., Lübbecke, J. F., Martin, T., Nnamchi, H. C., et al. (2023). Strengthening atmospheric circulation and trade winds slowed tropical Pacific surface warming. *Communications Earth & Environment*, *4*(1), 249. https://doi.org/10.1038/s43247-023-00912-4

Lee, S., L'Heureux, M., Wittenberg, A. T., Seager, R., O'Gorman, P. A., & Johnson, N. C. (2022). On the future zonal contrasts of equatorial Pacific climate: Perspectives from Observations, Simulations, and Theories. *npj Climate and Atmospheric Science*, *5*(1), 82. https://doi.org/10.1038/s41612-022-00301-2

Li, Q., Luo, Y., Lu, J., & Liu, F. (2024). Revisiting the equatorial Pacific sea surface temperature response to global warming. *Climate Dynamics*, *62*(3), 2239–2258. https://doi.org/10.1007/s00382-023-07019-8

Liu, Z., Philander, S. G. H., & Pacanowski, R. C. (1994). A GCM study of tropical–subtropical upper-ocean water exchange. *Journal of Physical Oceanography*, *24*(12), 2606–2623. https://doi.org/10.1175/1520-0485(1994)024<2606:agsotu>2.0.co;2

Long, D. J., & Collins, M. (2013). Quantifying global climate feedbacks, responses and forcing under abrupt and gradual CO2 forcing. *Climate Dynamics*, *41*(9), 2471–2479. https://doi.org/10.1007/s00382-013-1677-0

Luo, J.-J., Sasaki, W., & Masumoto, Y. (2012). Indian Ocean warming modulates Pacific climate change. *Proceedings of the National Academy of Sciences*, *109*(46), 18701–18706. https://doi.org/10.1073/pnas.1210239109

Luo, J.-J., Wang, G., & Dommenget, D. (2018). May common model biases reduce CMIP5's ability to simulate the recent Pacific La Niña-like cooling? *Climate Dynamics*, *50*(3), 1335–1351. https://doi.org/10.1007/s00382-017-3688-8

Luongo, M. T., Xie, S.-P., & Eisenman, I. (2022). Buoyancy forcing dominates the cross-equatorial ocean heat transport response to northern hemisphere extratropical cooling. *Journal of Climate*, *35*(20), 6671–6690. https://doi.org/10.1175/jcli-d-21-0950.1

Luongo, M. T., Xie, S.-P., Eisenman, I., Hwang, Y.-T., & Tseng, H.-Y. (2023). A pathway for northern hemisphere extratropical cooling to elicit a tropical response. *Geophysical Research Letters*, *50*(2), e2022GL100719. https://doi.org/10.1029/2022GL100719

Mechoso, C. R., Robertson, A. W., Barth, N., Davey, M. K., Delecluse, P., Gent, P. R., et al. (1995). The seasonal cycle over the tropical pacific in coupled ocean–atmosphere general circulation models. *Monthly Weather Review*, *123*(9), 2825–2838. https://doi.org/10.1175/1520-0493(1995)123<2825:tscott>2.0.co;2

Pauling, A. G., Bitz, C. M., Smith, I. J., & Langhorne, P. J. (2016). The response of the Southern Ocean and Antarctic sea ice to freshwater from ice Shelves in an Earth system model. *Journal of Climate*, *29*(5), 1655–1672. https://doi.org/10.1175/jcli-d-15-0501.1

Pausata, F. S. R., Zanchettin, D., Karamperidou, C., Caballero, R., & Battisti, D. S. (2020). ITCZ shift and extratropical teleconnections drive ENSO response to volcanic eruptions. *Science Advances*, *6*(23), eaaz5006. https://doi.org/10.1126/sciadv.aaz5006

Rodríguez-Fonseca, B., Polo, I., García-Serrano, J., Losada, T., Mohino, E., Mechoso, C. R., & Kucharski, F. (2009). Are Atlantic Niños enhancing Pacific ENSO events in recent decades? *Geophysical Research Letters*, *36*(20). https://doi.org/10.1029/2009GL040048

Rugenstein, M., Zelinka, M., Karnauskas, K., Ceppi, P., & Andrews, T. (2023). Patterns of surface warming matter for climate sensitivity. *Eos*, *104*. https://doi.org/10.1029/2023eo230411

Sadai, S., Condron, A., DeConto, R., & Pollard, D. (2020). Future climate response to Antarctic Ice Sheet melt caused by anthropogenic warming. *Science Advances*, *6*(39), eaaz1169. https://doi.org/10.1126/sciadv.aaz1169

Seager, R., Cane, M., Henderson, N., Lee, D.-E., Abernathey, R., & Zhang, H. (2019). Strengthening tropical Pacific zonal sea surface temperature gradient consistent with rising greenhouse gases. *Nature Climate Change*, *9*(7), 517–522. https://doi.org/10.1038/s41558-019-0505-x

Seager, R., Hoerling, M., Schubert, S., Wang, H., Lyon, B., Kumar, A., et al. (2015). Causes of the 2011–14 California drought. *Journal of Climate*, *28*(18), 6997–7024. https://doi.org/10.1175/jcli-d-14-00860.1

Sobel, A. H., Lee, C.-Y., Bowen, S. G., Camargo, S. J., Cane, M. A., Clement, A., et al. (2023). Near-term tropical cyclone risk and coupled Earth system model biases. *Proceedings of the National Academy of Sciences*, *120*(33), e2209631120. https://doi.org/10.1073/pnas.2209631120

Takahashi, C., & Watanabe, M. (2016). Pacific trade winds accelerated by aerosol forcing over the past two decades. *Nature Climate Change*, *6*(8), 768–772. https://doi.org/10.1038/nclimate2996

Tian, B., & Dong, X. (2020). The double-ITCZ bias in CMIP3, CMIP5, and CMIP6 models based on annual mean precipitation. *Geophysical Research Letters*, *47*(8), e2020GL087232. https://doi.org/10.1029/2020GL087232

Trenberth, K. E., Branstator, G. W., Karoly, D., Kumar, A., Lau, N.-C., & Ropelewski, C. (1998). Progress during TOGA in understanding and modeling global teleconnections associated with tropical sea surface temperatures. *Journal of Geophysical Research*, *103*(C7), 14291–14324. https://doi.org/10.1029/97JC01444

Tseng, H.-Y. (2024). Data_Tseng_et_al._2024_GRL [Dataset]. *figshare*. https://doi.org/10.6084/m9.figshare.26879446.v1

Tseng, H.-Y., Hwang, Y.-T., Xie, S.-P., Tseng, Y.-H., Kang, S. M., Luongo, M. T., & Eisenman, I. (2023). Fast and slow responses of the tropical pacific to radiative forcing in northern high latitudes. *Journal of Climate*, *36*(16), 5337–5349. https://doi.org/10.1175/jcli-d-22-0622.1

Vecchi, G. A., & Soden, B. J. (2007). Global warming and the weakening of the tropical circulation. *Journal of Climate*, *20*(17), 4316–4340. https://doi.org/10.1175/jcli4258.1

Wang, C.-C., Lee, W.-L., & Chou, C. (2019). Climate effects of anthropogenic aerosol forcing on tropical precipitation and circulations. *Journal of Climate*, *32*(16), 5275–5287. https://doi.org/10.1175/jcli-d-18-0641.1

Wills, R. C. J., Dong, Y., Proistosecu, C., Armour, K. C., & Battisti, D. S. (2022). Systematic climate model biases in the large-scale patterns of recent sea-surface temperature and sea-level pressure change. *Geophysical Research Letters*, *49*(17), e2022GL100011. https://doi.org/10.1029/2022GL100011

Xie, S.-P., Deser, C., Vecchi, G. A., Ma, J., Teng, H., & Wittenberg, A. T. (2010). Global warming pattern formation: Sea surface temperature and rainfall. *Journal of Climate*, *23*(4), 966–986. https://doi.org/10.1175/2009jcli3329.1

You, Y., & Furtado, J. C. (2018). The South pacific meridional mode and its role in tropical pacific climate variability. *Journal of Climate*, *31*(24), 10141–10163. https://doi.org/10.1175/jcli-d-17-0860.1

Zhang, H., Clement, A., & Di Nezio, P. (2014). The South pacific meridional mode: A mechanism for ENSO-like variability. *Journal of Climate*, *27*(2), 769–783. https://doi.org/10.1175/jcli-d-13-00082.1

Zhang, H., Deser, C., Clement, A., & Tomas, R. (2014). Equatorial signatures of the pacific meridional modes: Dependence on mean climate state. *Geophysical Research Letters*, *41*(2), 568–574. https://doi.org/10.1002/2013GL058842

Zhang, L., Sun, D.-Z., & Karnauskas, K. B. (2019). The role of the Indian Ocean in determining the tropical pacific SST response to radiative forcing in an idealized model. *Dynamics of Atmospheres and Oceans*, *86*, 1–9. https://doi.org/10.1016/j.dynatmoce.2019.02.003

Zhang, X., Deser, C., & Sun, L. (2021). Is there a tropical response to recent observed Southern Ocean cooling? *Geophysical Research Letters*, *48*(5), e2020GL091235. https://doi.org/10.1029/2020GL091235

Zhang, X., Liu, H., & Zhang, M. (2015). Double ITCZ in coupled ocean-atmosphere models: From CMIP3 to CMIP5. *Geophysical Research Letters*, *42*(20), 8651–8659. https://doi.org/10.1002/2015GL065973

PNAS RESEARCH ARTICLE | EARTH, ATMOSPHERIC, AND PLANETARY SCIENCES OPEN ACCESS

Contribution of anthropogenic aerosols to persistent La Niña-like conditions in the early 21st century

Yen-Ting Hwang[a,1], Shang-Ping Xie[b], Po-Ju Chen[a,c], Hung-Yi Tseng[a], and Clara Deser[d,1]

Contributed by Clara Deser; received September 8, 2023; accepted December 8, 2023; reviewed by Kay McMonigal and Michael J. McPhaden

The discrepancy between the observed lack of surface warming in the eastern equatorial Pacific and climate model projections of an El Niño-like warming pattern confronts the climate research community. While anthropogenic aerosols have been suggested as a cause, the prolonged cooling trend over the equatorial Pacific appears in conflict with Northern Hemisphere aerosol emission reduction since the 1980s. Here, using CESM, we show that the superposition of fast and slow responses to aerosol emission change—an increase followed by a decrease—can sustain the La Niña-like condition for a longer time than expected. The rapid adjustment of Hadley Cell to aerosol reduction triggers joint feedback between low clouds, wind, evaporation, and sea surface temperature in the Southeast Pacific, leading to a wedge-shaped cooling that extends to the central equatorial Pacific. Meanwhile, the northern subtropical cell gradually intensifies, resulting in equatorial subsurface cooling that lasts for decades.

climate change | atmosphere–ocean interaction | climate teleconnection | sea surface temperature pattern

Significance

The tropical Pacific plays a crucial role in global energy and moisture distribution, and accurate prediction of its changes is vital for society's adaptation to growing climate change. The cause of surface cooling trends observed over the past 40 y in the tropical eastern Pacific eludes a satisfactory explanation. Our study shows that anthropogenic aerosol effects on the equatorial Pacific Ocean may have reached a peak and that the response features a La Nina-like cooling pattern. Prolonged aerosol influence is clarified through dual timescale responses involving air–sea flux and ocean dynamics.

The sea surface temperature (SST) anomaly pattern in the tropical Pacific has significant influence on global weather and climate. Over the past four decades, the equatorial cold tongue has cooled while the rest of the tropics have warmed (1), modulating the pace of global surface warming (2, 3), amplifying tropical cyclone genesis over the Northwest Pacific (4), and heightening the likelihood of drought occurrence in the western United States (5). The aforementioned trends might cease or even reverse if the cold tongue warms up and Walker Cell weakens, as anticipated by climate models. How the tropical Pacific may change under anthropogenic forcing has been a subject of active debate for decades and is still ongoing. The complex interplay among global dynamics, air–sea interactions, and radiative processes has given rise to multiple unresolved conundrums, including the interpretation of the observed trend, the discrepancy between models and observations (1, 6), and diverging theories (6, 7).

One plausible interpretation for the observed eastern tropical Pacific cooling trend, particularly during the early 2000s, is that it is predominantly driven by internal variability, either through the negative phase of Pacific Decadal Variability (PDV) (2, 8–13) or the decadal variation of independent ENSO events (14–16). Despite accounting for a range of internal variability, it remains uncommon to find historical simulations with fully coupled climate models that accurately replicate the strengthening of the zonal SST gradient observed over the past 50 y (1, 6). Furthermore, the cooling trend observed in the subtropical South Pacific and equatorial eastern Pacific has persisted despite the transition toward a positive PDV phase after 2013, prompting the need for an alternative explanation, namely that a portion of the observed trend may be driven by external forcing that current models fail to simulate adequately.

The exploration of idealized experiments, which enable the decomposition of the complex response to increasing carbon dioxide (CO_2) into a fast and a slow component, has yielded significant insights (17–19). The fast component closely aligns with the observed trend (20) and the "ocean thermostat" hypothesis (21). This stands in stark contrast to the slow component, which exhibits a reduced zonal gradient consistent with long-term model projections and the thermodynamic constraints imposed by radiative cooling (22) and evaporative damping (23, 24). The framework of multiple timescale responses offers a promising avenue for resolving discrepancies between models and observations, as well as reconciling the various competing mechanisms at play in this intricate system (19, 25). It is hypothesized that the strength of the ocean thermostat may be underestimated by current models, and the enhanced warming over the equatorial cold tongue may eventually manifest (19, 25).

Evidence from single forcing experiments indicates that anthropogenic aerosols exert a comparable influence to greenhouse gases in shaping the SST pattern during the

Author affiliations: [a]Department of Atmospheric Sciences, National Taiwan University, Taipei 10617, Taiwan; [b]Scripps Institute of Oceanography, University of California San Diego, La Jolla, CA 92093; [c]Department of Atmospheric, Oceanic, and Earth Sciences, George Mason University, Fairfax, VA 22030; and [d]Climate and Global Dynamics Division, National Center for Atmospheric Research, Boulder, CO 80305

Author contributions: Y.-T.H. designed research; P.-J.C. and H.-Y.T. performed research; C.D. contributed new reagents/analytic tools; Y.-T.H., P.-J.C., and H.-Y.T. analyzed data; S.-P.X. provided important insights for interpreting the results and forming the article's storyline; C.D. provided important insights for interpreting the results; and Y.-T.H., S.-P.X., and C.D. wrote the paper.

Reviewers: K.M., University of Alaska Fairbanks; and M.J.M., National Oceanic and Atmospheric Administration Pacific Marine Environmental Laboratory.

The authors declare no competing interest.

[1]To whom correspondence may be addressed. Email: ythwang@ntu.edu.tw or cdeser@ucar.edu.

This article contains supporting information online at https://www.pnas.org/lookup/suppl/doi:10.1073/pnas.2315124121/-/DCSupplemental.

Published January 22, 2024.

observational period (26–32). However, our current understanding of the Earth system's responses to anthropogenic aerosols on different timescales remains limited (33), hindering our ability to accurately attribute past climate change and assess uncertainties in climate change projections. For instance, a notable reduction in aerosol concentrations has already been observed in North America and Europe since 1980, as well as in East Asia since 2000. Naively predicting that the decrease in aerosols would lead to a weakening of the observed La Niña-like SST pattern trend appears to contradict both the available observational records and the outcomes of single forcing simulations.

In the following, we explore the possible role of non-monotonic evolution of anthropogenic sulfate aerosols in slowing down the equatorial Pacific warming. Our findings reveal that the equatorial Pacific response to aerosol radiative forcing exhibits distinct fast and slow components. We then put forth a hypothesis that these components interact and result in an equatorial cooling that is stronger in the early 21st century than in the 1980s. The superposition of the fast and slow response to the Northern Hemisphere sulfate aerosol emission trajectory, which consists of an increase followed by a decrease, may sustain the La Niña-like SST pattern for an extended duration that is longer than previous estimations.

The Experimental Design

We differentiate the fast and slow components of the climate system's response to anthropogenic aerosols by conducting a 15-ensemble-member step function experiment using the Community Earth System Model version 1 (CESM1) at 2° resolution for the atmosphere and land components and 1° resolution for the ocean and sea ice components. The last-millennium ensemble (34) and the CMIP5 archive also utilized the same version and resolution, identified as "CESM1 (CAM5.1, FV2)." Note that the CESM1 model at 2° resolution is particularly skillful in simulating some of the key processes involved in the response, including low cloud-SST feedback (35) and the Pacific mean state (36). The experiment consists of suddenly introducing and then maintaining a constant pattern of sulfate aerosol emissions representative of 1980s levels taken from CMIP5 historical forcing data (*SI Appendix*, Fig. S1*A*) for the first 30 y of the simulation, followed by an abrupt return to pre-industrial (year 1850) levels for an additional 30 y. Ensemble members are generated by initializing the experiments by the conditions on January 1st of the last 15 consecutive years in the control simulation. The evolving forced response anomaly is calculated by subtracting the climatology of the 90-y pre-industrial control simulation from the average of the 15 ensemble members. Detailed definitions for the fast and slow components of aerosol emission and aerosol removal can be found in the *Methods*. The fast and slow components of the SST response are very similar to those obtained with a similar set of experiments using the 2020s distribution of sulfate aerosol emissions (*SI Appendix*, Fig. S1 *D* and *F*). The similarity implies that the proposed mechanisms shaping the fast and slow components of SST response are operating across both historical simulations and future projections, despite the different patterns of aerosol emissions.

Multiple Timescale Responses in the Equatorial Pacific Region

The equatorial Pacific, located far from the Northern Hemisphere aerosol emission source regions, shows a clear indication of a multiple timescale response. The imposed step-function in aerosol emissions results in a complex evolution of oceanic temperatures, as shown in Fig. 1. Initially (within the first 3 y), SSTs in the central and eastern equatorial Pacific SST undergo warming before transitioning to cooling thereafter (Fig. 1*A*). It is notable that the maximum cooling takes place in the 3 y immediately following the abrupt cessation of aerosol forcing at year 30 (Fig. 1*A*). Although the surface cooling gradually decreases after year 35, subsurface cooling persists for decades after the radiative forcing has been removed (Fig. 1*B*). Additionally, the subsurface cooling reaches maximum strength during years 33 to 45, after the aerosol emissions return to preindustrial levels. Both the surface and subsurface signals indicate a persistent cooling long after the aerosol emissions are abruptly terminated.

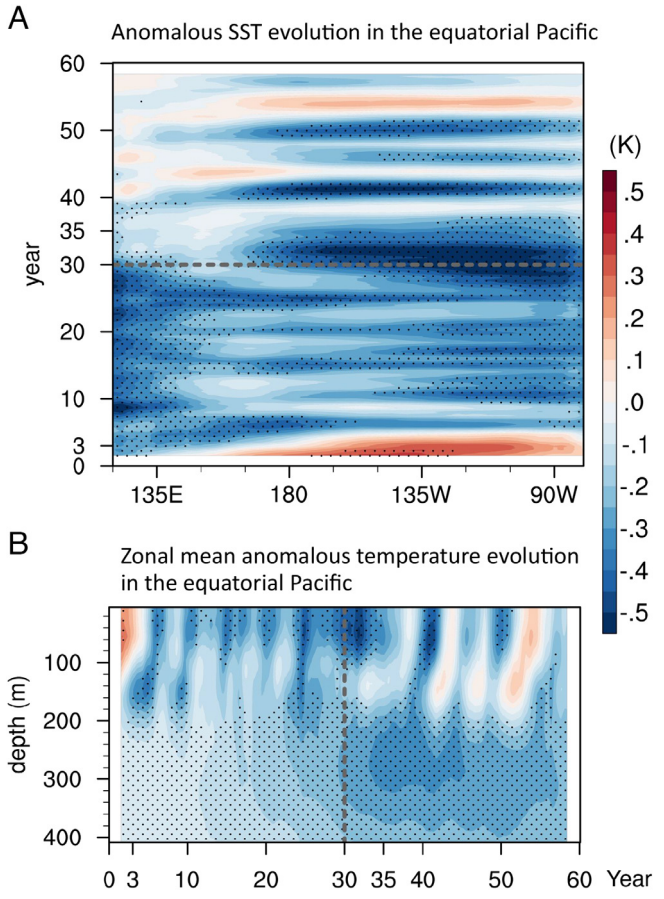

Fig. 1. Temporal evolutions of anomalous oceanic temperature in the idealized aerosol experiments relative to the climatology in the control simulation. (*A*) The 3-y running mean of meridionally averaged SST anomalies in the equatorial Pacific (5°S~5°N). (*B*) The 3-y running mean of the equatorial Pacific temperature response which is zonally and meridionally averaged (5°S~5°N; Pacific basin). Dotted region indicates statistically significant values of temperature anomalies at the 95% confidence level based on two-sided *t* test.

The multiple timescale responses identified in the idealized experiments can also be seen in a more realistic setting. Fig. 2 compares the Niño3.4 index and subsurface ocean temperature in the equatorial Pacific for both the idealized step function experiment and the standard CESM experiments with realistic emission scenarios (historical and RCP8.5) (29) (*Methods*). The average global aerosol emission reaches its highest point around 1970 to 1990, causing the Niño3.4 region's SST and subsurface temperature to experience cooling that show little sign of weakening even after year 1990. The equatorial subsurface cooling reaches maximum strength several decades after the aerosol emissions peak. According to the CESM single forcing experiment, we are about to experience the peak equatorial subsurface cooling (around year 2030 to 2050) induced by aerosols.

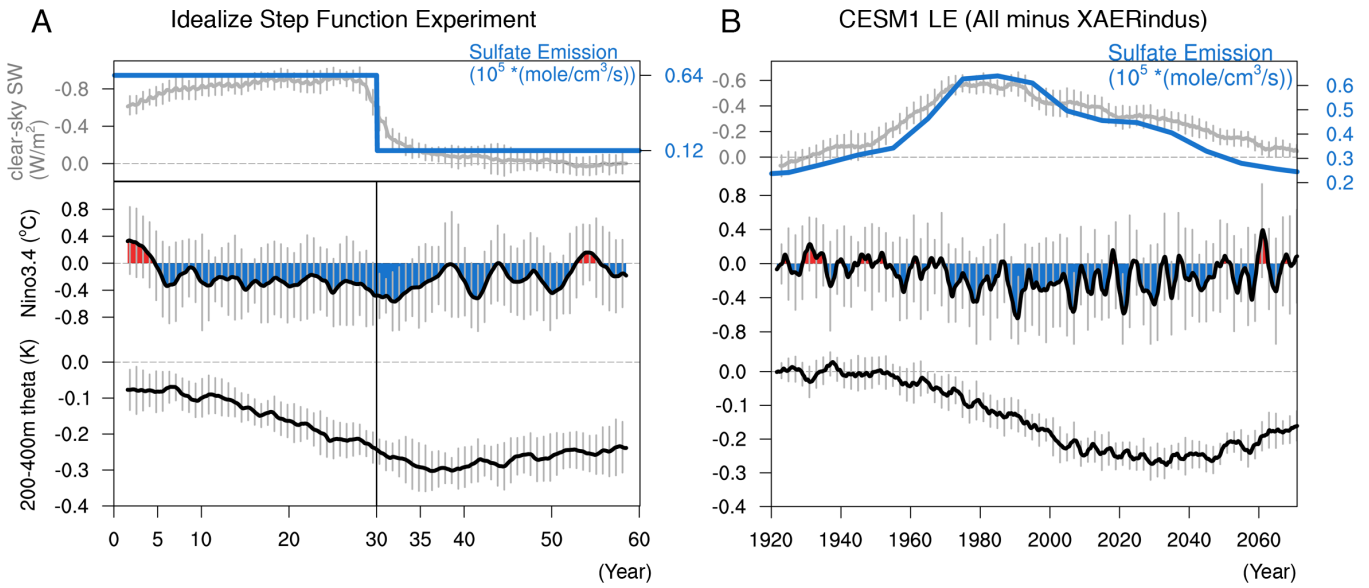

Fig. 2. Temporal evolutions of imposed sulfate aerosol emissions and equatorial Pacific climate response. *Top* row: the global mean sulfate emission imposed in the idealized experiment (*A*) and CESM LE All minus XAERindus (*B*). The gray lines denote the global mean anomalous SW radiation in clear sky. *Middle* and *Bottom* rows: the evolutions of averaged SST in the Niño3.4 region (5°S~5°N; 170°W~120°W) and averaged potential temperature in the subsurface equatorial Pacific (200 to 400 m; 5°S~5°N; Pacific basin) in the idealized experiment (*Left*) and CESM-LE (*Right*). All indices except the global mean sulfate emission are smoothed by 3-y running mean in the idealized experiment and by a 5-y running mean in CESM-LE. The thick black curves and the thin gray bars indicate the ensemble mean and the 1 SD among ensemble members, respectively.

In the following, we utilize the idealized experiment to investigate the distinct characteristics and underlying mechanisms behind the fast and slow elements of the climatic response to anthropogenic aerosol forcing. The multiple timescale elements explain why the peak aerosol influence on the tropical Pacific occurs after emission reduction.

The Fast Component

The fast component reveals a remote influence of aerosols that has the opposite sign from that expected from the imposed forcing, a phenomenon that has yet to be recognized in the existing literature. In the case of aerosol emissions, this manifests as a wedge-shaped SST warming pattern reaching its maximum intensity in the central equatorial Pacific, extending southeastward, and featuring a sharp front north of the equator (Fig. 3*A*). The reduced equatorial zonal SST gradient and easterlies are associated with a flatten thermocline and a typical seesaw temperature anomaly in the equatorial band (Fig. 3*C*). Here, we disentangle how the anomalous radiative forcing, primarily concentrated in the northern extratropics, gives rise to a remote SST response in the equatorial Pacific with an opposite sign from that expected from the forcing. In the *Summary and Outlook*, we will discuss how the same pattern with reversed sign explains the enhanced cooling

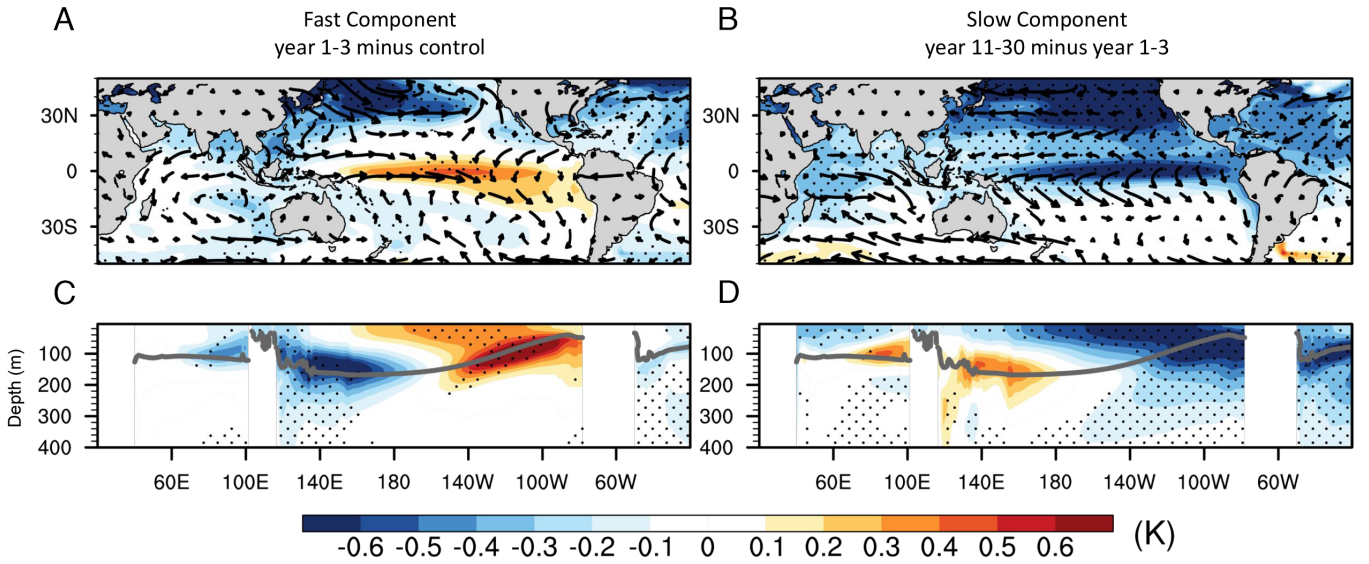

Fig. 3. The fast and slow responses in the idealized aerosol experiments. (*A* and *B*) Spatial patterns of SST (shaded) and surface wind stress (vector) anomalies. (*C* and *D*) Vertical structure of potential temperature anomalies along the equator (5°S~5°N mean) as a function of depth (m). Dotted region indicates statistically significant values of temperature anomalies at the 95% confidence level based on two-sided *t* test.

that takes place after the sudden removal of aerosol emissions in our idealized experiment and contributes to the La Niña-like trend in more realistic simulations (and by extension the observed trends).

We propose that the formation of the cross-equatorial Hadley Cell, along with its associated air–sea interactions, drives the observed teleconnection pattern in the tropical Pacific. The energetic framework (37–39) offers a plausible interpretation for the development of this anomalous cross-equatorial cell. In response to aerosol emissions, an anomalous cross-equatorial cell emerges, transporting energy toward the north (Figs. 4 *A* and *B* and 5*A*). The accompanying pattern of surface winds plays a pivotal role in establishing the SST pattern in the tropical Pacific, as described below.

First, the meridional winds in the equatorial eastern Pacific hold a significant influence over thermocline depth and the strength of the cold tongue (40). A reduction in the trade winds across the equator suppresses mixing, limits upwelling, and results in a flatter thermocline (Fig. 3*C*). Despite very little radiative forcing in the tropics, the anomalous cross-equatorial winds that are generated remotely by aerosols in the northern extratropics can induce a tropical SST response that resembles the dynamical thermostat mechanism frequently discussed in the context of greenhouse warming or volcanic eruptions (19, 21, 25, 41, 42). We confirm the key role of extratropical aerosols via performing additional experiment that only considers tropical aerosol emissions, which does not enable the dynamical thermostat mechanism and displays a slight equatorial cooling instead for the fast response [see *SI Appendix*, Fig. S2, contrary to the hypothesis presented in Verma et al. (33) based on year 2000 emissions].

Second, the anomalous cross-equatorial winds strengthen the trade winds in the northern tropics and weaken them in the southern tropics. Weakened trades in the south inhibit coastal upwelling, diminish stratus and stratocumulus clouds along the coast of South America, and reduce the east-west SST gradient in the subtropics. Given that the climatological rainband is located north of the equator, the combined wind-evaporation-SST and low cloud-SST feedbacks can spread anomalous warming from the Southeast Pacific to the equatorial central and eastern Pacific (43–46) (Fig. 3*A*). Meanwhile, the anomalous cooling caused by strengthened trades and the joint wind-evaporation-low cloud-SST feedback is blocked by the rainband. It can only enter the equatorial region from the west. The resulting weakened zonal SST gradient in the equatorial western-central Pacific reduces the easterlies, thereby reducing zonal cold advection and meridional Ekman energy divergence. This, in turn, further amplifies the warming (47) (see Fig. 4*D* for the anomalous deep tropical subtropical cell (STC) driving the Ekman energy convergence and *SI Appendix*, Fig. S3 for the energy budget analysis of the upper 0 to 50 m).

The Slow Component

The slow component of the climate response to aerosol forcing exhibits an enhanced equatorial zonal SST gradient and an intensification of the Walker Cell, consistent with the literature (26, 28, 48) (Fig. 3*B*). The cooling of the slow component extends well below the thermocline to at least 400 m depth. Intriguingly, these surface and subsurface cooling anomalies in the equatorial region occur within decadal timescale and show little sign of recovery after aerosol removal (Fig. 1), a phenomenon previously unreported in the literature. In this section, we delve into the ocean dynamical mechanisms that drive the spread of aerosol-induced cooling to the equatorial region. The persistent nature of this oceanic response emphasizes the potential to detect the cooling anomalies in the noisy observational records, which we compare with the historical simulations in the last section.

We propose that the interhemispherically asymmetric surface wind anomalies and the associated air–sea interactions in the fast response drive the slow oceanic adjustments and set the stage for

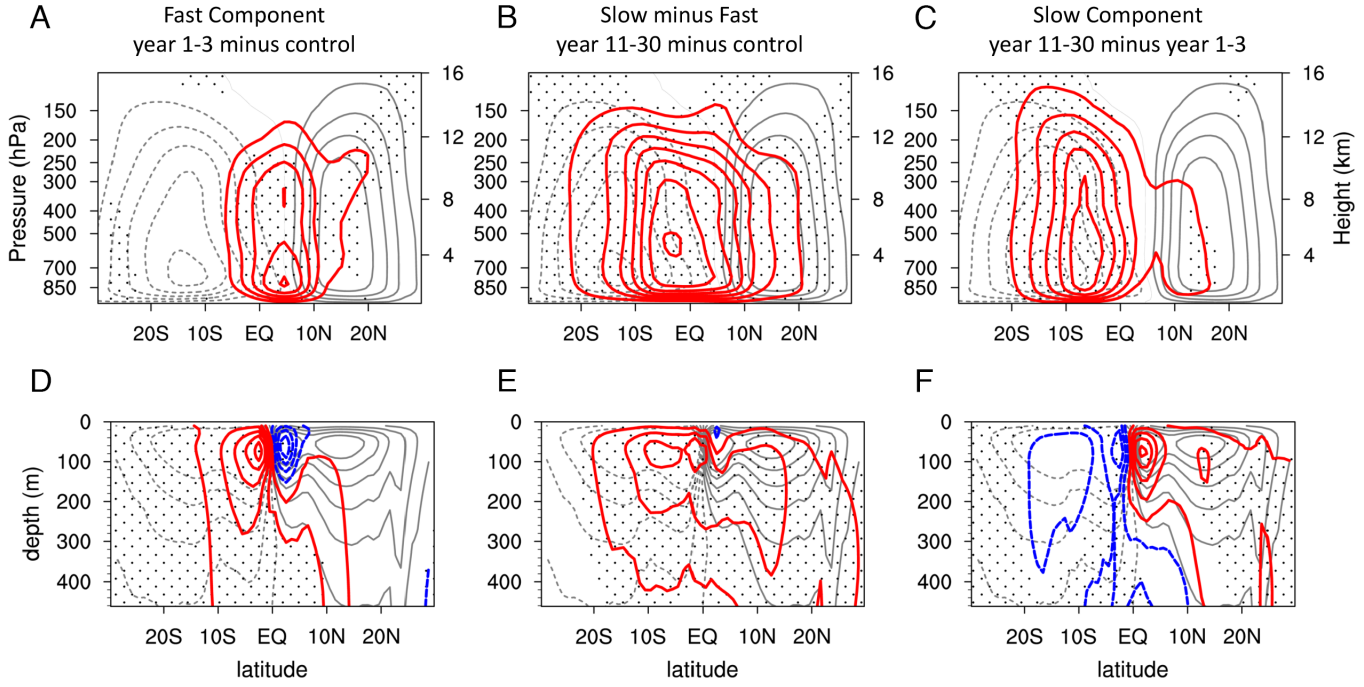

Fig. 4. Climatological (gray contours) and anomalous (colored contours) meridional mass streamfunction in the atmosphere (*A*–*C*) and in the Indo-Pacific ocean (*D*–*F*). Dotted region indicates statistically significant values of anomalies at the 95% confidence level based on two-sided *t* test. The contour intervals for panels (*A*–*C*) are 2×10^{10} m^3/s for climatology and 2×10^9 m^3/s for anomalies. For (*D*–*F*), the contour intervals are 4 Sv for climatology and 0.8 for anomalies.

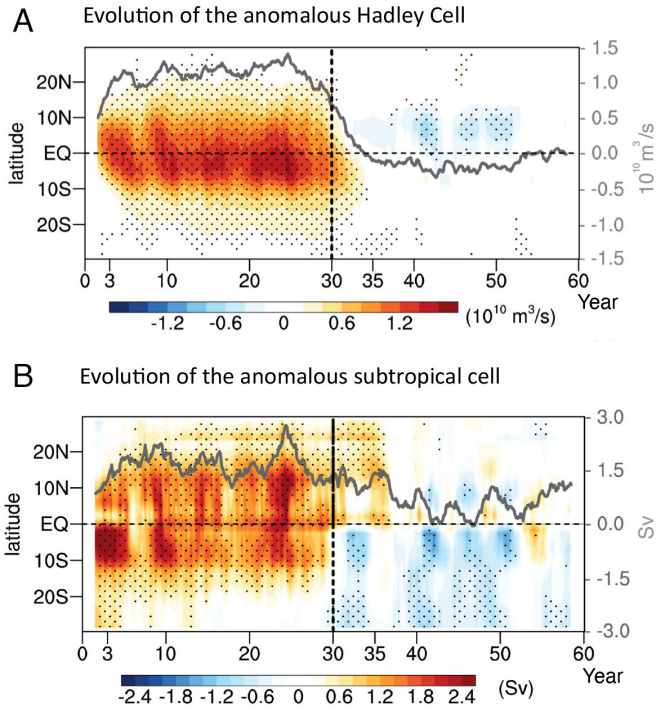

Fig. 5. Temporal evolutions of anomalous meridional circulations and their indices in the idealized aerosol experiments. The timeseries are all smoothed by a 3-y running mean. (*A*) displays the change in Hadley Cell (shaded) which is shown by the vertically averaged mass streamfunction (globally zonal mean; 300 to 700 hPa). The positive anomalies indicate anomalous northward flows in the upper level and southward flows in the lower level, vice versa. The solid line denotes the strength of anomalous cross-equatorial Hadley Cell using the mass streamfunction averaged over the domain (10°S~10°N; 300 to 700 hPa). (*B*) displays the change in the Meridional Overturning Circulation in the tropical Pacific (shaded) through the vertically averaged mass streamfunction (100 to 300 m). The solid line represents the index of the strength which is the maximum of the Meridional Overturning Circulation in a domain (10°N~30°N; 0 to 400 m). Dotted region indicates statistically significant values of anomalous mass streamfunction at the 95% confidence level based on two-sided *t* test.

the slow response. Since oceanic temperature and circulation respond slowly, the resulting equatorial cooling does not become significant until year 10 (Fig. 1*A*). Also, the removal of the aerosol forcing does not result in an immediate recovery of oceanic circulation, as shown below.

The so-called "oceanic tunnel" provides a linkage for the Northern Hemisphere extratropical SST cooling of the fast response to the tropical ocean (45, 49, 50). That is, the aerosol cooling and the associated joint low cloud-WES feedback lower the temperature of waters subducted within the STC, causing colder water to be advected downward and equatorward. Indeed, we observe cooler water penetrating into the oceanic interior in the eastern Pacific basin around 20~30°N and transporting equatorward to 15°N a few years after the imposition of aerosol forcing (*SI Appendix*, Fig. S4).

Targeting the equatorial Pacific oceanic energy budget, the loss of energy and the resultant cooling in the equatorial Pacific Ocean are mainly caused by changes in the northern STC (refer to *SI Appendix*, Fig. S5 for changes in meridional energy convergence dominating energy budgets of 0 to 200 m and 0 to 400 m and see *SI Appendix*, Fig. S6 for $V'\overline{T}$ of the northern boundary outweighing other terms). The cooling in the northern mid-latitudes leads to an increase in subtropical wind stress and wind-stress curl, which then spins up the Pacific Gyre circulation and, as a result of the Sverdrup balance, strengthens the northern STC (Figs. 4*E* and 5*B*). The northern STC intensifies within 2 to 3 y of imposing aerosol forcing, matching the time for baroclinic Rossby waves to cross the Pacific Basin (51, 52). In addition to the wind-driven mechanism, the aforementioned anomalous cooling introduced by the oceanic tunnel can reinforce and extend the intensified STC via altering density and vertical stability (53). The strengthened northern STC reaches its peak at year 10 and persists for more than 10 y after switching off aerosol emissions, leading to a continued export of energy and a gradually intensified cooling in the equatorial region (54). The cooler equatorial water is upwelled from the cold tongue, kicking off a series of air–sea interactions and leading to a persistent La Niña-like condition.

Summary and Outlook

We have examined the fast and slow components of tropical Pacific SST responses to anthropogenic sulfate aerosol emissions. We observe that the equatorial Pacific displays opposing signs of fast and slow components, and both components are insensitive to exact aerosol distributions outside the equatorial region. As summarized in Fig. 6, the unique patterns of both surface fast and subsurface slow responses reinforce each other, resulting in a notably strong equatorial cooling that persists decades after the removal of anthropogenic aerosols. Following an abrupt removal of aerosols, the Hadley Cell responds quickly (Figs. 5*A* and 6*A*). The intensified trades, the associated coastal Ekman upwelling, and the chain of low cloud-WES feedback processes, lead to a cooling trend in the southeast Pacific extending toward the equatorial central Pacific. The anomalous northern STC, which is the signature of the slow response of aerosol increase, persists for a few more years after the aerosol removal (Figs. 5*B* and 6*B*). This, in turn, results in a continued cooling trend in the equatorial subsurface. The surface air–sea interactions associated with the rapid Hadley Cell adjustment and the prolonged anomalous energy transport divergence in the ocean interior caused by the continuous northern STC strengthening both contribute constructively to the La Niña-like condition.

The characteristics of the two distinct components of response can be seen in simulations conducted under more realistic conditions, as well as in the observed trend. The fast response, which lasts only a few years in the idealized experiment, transforms into a continuous linear trend in the simulations with realistic aerosol emission trajectories, which exhibit increasing and decreasing trends lasting for decades. Notably, the greatest spatial correlation between the fast component identified in the idealized experiment and the linear trends observed in the CESM LE single forcing experiment is found during the 1960s—a decade marked by a substantial increase in Northern Hemisphere aerosol emissions (*SI Appendix*, Fig. S7). Conversely, La Niña-like trends emerge in the 1990s, coinciding with a more pronounced reduction in aerosol emissions in the CESM LE single forcing experiment. During 1981 to 2000, the period characterized by rapid interhemispherically asymmetric changes in SST, the spatial correlation between the fast component and the observed SST trend reaches −0.63 (*SI Appendix*, Fig. S7). Furthermore, the persistent cooling of the equatorial subsurface—a characteristic feature of the slow response—can be seen not only in the single forcing experiment but also in the standard historical simulation considering GHG warming and the reanalysis data (*SI Appendix*, Fig. S8).

Our findings are based on a single model (CESM), and the temporal and spatial characteristics of the two components identified here remain to be tested and compared with other models

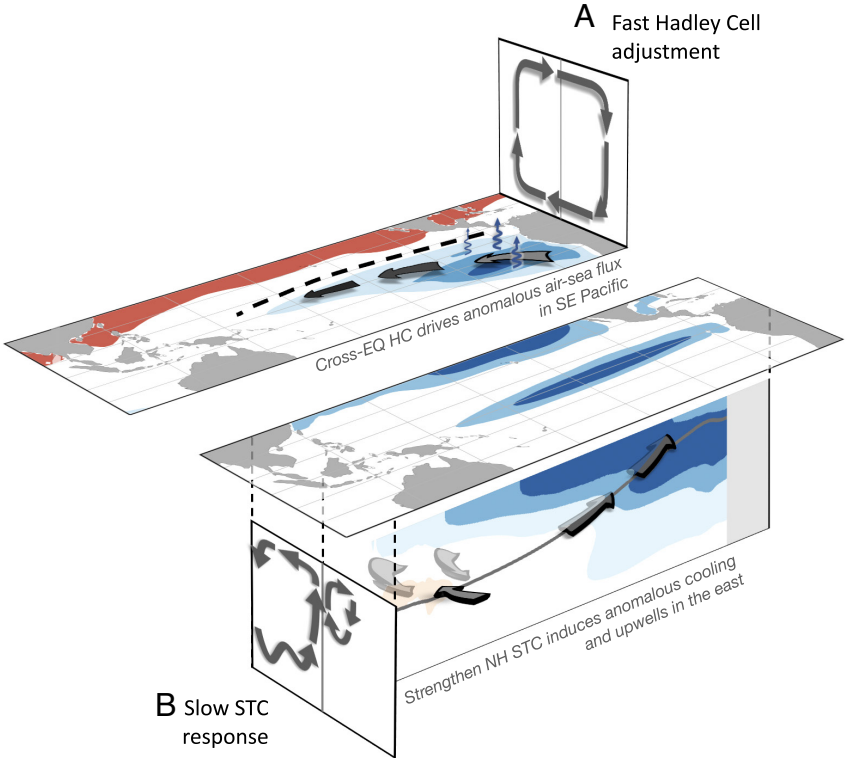

Fig. 6. A schematic illustrating the distinct characteristics of and the interplay between the fast component of aerosol emission reduction and the slow component of aerosol emission increase. Shadings represent anomalous oceanic potential temperature. Arrows in the two vertical planes are the anomalous cross-equatorial Hadley Cell and the anomalous oceanic STC. The thick arrows in the *Top* panel A illustrates intensified trades and the thin blue arrows illustrate the associated air-sea fluxes. The thick arrows in the *Bottom* panel B illustrate how the intensified STC induces cold water, which converges in west Pacific subtropics and upwells in the east.

and different emission scenarios. Despite the caveat, the mechanistic understanding of the two components reported here provides valuable insights for unraveling the discrepancies between global climate model simulations and observational records. For instance, the well-known double ITCZ biases, characterized by the presence of the eastern Pacific rainband in the southern hemisphere for a longer duration compared to the real world, can hinder the connection between the southern subtropics and the equatorial region in the fast component. In some global climate models, the spurious rainband obstructs the chain of air–sea interaction that typically brings the anomalous cooling from the South Pacific to the equatorial region. Furthermore, the underestimation of the strength of the stratus cloud-SST feedback, a bias common to most global climate models [but not the two-degree CESM1 that we use (35)], also impacts the relationship between SSTs in the southeast and equatorial Pacific. Turning to the slow response, biased low stratus cloud-SST feedbacks in the northern subtropics contribute to an inaccurate estimation of weakening in the STC and the resulting equatorial cooling. Additionally, global climate models tend to exhibit excessive stratification in the equatorial Pacific, impeding the upwelling of STC-induced cooling in the eastern equatorial Pacific. A process-based understanding of model biases is crucial for improved regional climate projections.

The implications of the proposed Hadley circulation and STC responses to an interhemispheric thermal gradient extend beyond the simulated effects of anthropogenic sulfate aerosols. The intensified warming trend observed in the mid-to-high latitudes of the Northern Hemisphere and the muted warming in the Southern Ocean, regardless of whether the causes are aerosol recovery, greenhouse gas-induced warming, or ozone depletion, could potentially trigger similar adjustments in the Hadley Cell, air–sea interaction, and STC. Although our study primarily focuses on the prolonged La Niña-like cooling trend, the accelerated warming over the Southern Ocean and the subtropical oceanic interior would engender a reverse mechanism and an El Niño-like background state in the future. Additionally, the circulation adjustments across multiple timescales and their impacts on the mean state of the tropical Pacific will also influence tropical climate variability, such as the El Niño/Southern Oscillation.

Methods

Definitions of the Fast and Slow Components. We define the fast components as the average of years 1 to 3 minus control and the average of years 31 to 35 minus years 11 to 20 (Fig. 3*A* and *SI Appendix*, Fig. S1*C*), based on the evolution of the Niño 3.4 index (Fig. 2*A*). The slow components are defined as the average of years 11 to 20 minus years 1 to 3 and the average of years 41 to 60 minus years 31 to 35 (Fig. 3*B* and *SI Appendix*, Fig. S1*E*). Through subtracting the fast component, the slow component partly excludes the cross-equatorial Hadley Cell response that develops quickly and highlights the enhanced equatorial response that is hemispherically symmetric. The overall patterns are not sensitive to the choice of the definitions, although the absolute anomalies are.

CESM Single Forcing Large Ensemble. To evaluate the climate responses to aerosol forcing with realistic temporal and spatial variations, we take the difference between the 40-member CESM large ensemble all forcing experiment (55) and the 20-member "XAERindus" experiment from the CESM single forcing large ensemble (29). The "XAERindus" uses the same forcing protocol as the all forcing experiment, i.e., the CMIP5 historical and RCP8.5 forcing protocols, except that the industrial anthropogenic aerosols' emission is held fixed at 1920 conditions. The model used in the CESM all forcing and single forcing large ensemble is the same as that of the idealized step function aerosol experiment used in this study but at a higher resolution (1°).

Data, Materials, and Software Availability. All processed data to support the analysis and figure codes publicly available at https://doi.org/10.6084/m9.figshare.24581016 (56). Data from CESM1 Single Forcing Large Ensemble Project is publicly available at: https://www.cesm.ucar.edu/working-groups/climate/simulations/cesm1-single-forcing-le (29). Monthly outputs from the idealized aerosol experiments are available from Y.-T.H. on request.

ACKNOWLEDGMENTS. S.-P.X. is sponsored by NSF AGS 2105654, C.D. by the NSF under Cooperative Agreement 1852977. Y.-T.H., P.-J.C., and H.-Y.T. are supported by Ministry of Science and Technology of Taiwan (MOST 110-2628-M-002-002, MOST 111-2628-M-002-003-, and NSTC 112-2111-M-002-016-MY4). We thank Hsing-Hung Chou for making the schematic (Fig. 6), Po-Chun Chung and Wan-Yu Wu for their help at the initial stage of the project, Kun Wang for sharing the codes for budget analysis, M.J.M. and K.M. for their constructive comments, and John Chiang and Yu-Heng Tseng for valuable discussions.

1. R. C. J. Wills, Y. Dong, C. Proistosecu, K. C. Armour, D. S. Battisti, Systematic climate model biases in the large-scale patterns of recent sea-surface temperature and sea-level pressure change. *Geophys. Res. Lett.* **49**, e2022GL100011 (2022).
2. Y. Kosaka, S.-P. Xie, Recent global-warming hiatus tied to equatorial Pacific surface cooling. *Nature* **501**, 403–407 (2013).
3. T. Andrews *et al.*, On the effect of historical SST patterns on radiative feedback. *J. Geophys. Res. Atmos.* **127**, e2022JD036675 (2022).
4. C. Zhao *et al.*, Enlarging rainfall area of tropical cyclones by atmospheric aerosols. *Geophys. Res. Lett.* **45**, 8604–8611 (2018).
5. R. Seager *et al.*, Causes of the 2011–14 California drought. *J. Clim.* **28**, 6997–7024 (2015).
6. S. Lee *et al.*, On the future zonal contrasts of equatorial Pacific climate: Perspectives from observations, simulations, and theories. *npj Clim. Atmos. Sci.* **5**, 82 (2022).
7. U. K. Heede, A. V. Fedorov, N. J. Burls, Time scales and mechanisms for the tropical Pacific response to global warming: A tug of war between the ocean thermostat and weaker walker. *J. Clim.* **33**, 6101–6118 (2020).
8. M. H. England *et al.*, Recent intensification of wind-driven circulation in the Pacific and the ongoing warming hiatus. *Nat. Clim. Change* **4**, 222–227 (2014).
9. M. Watanabe, J.-L. Dufresne, Y. Kosaka, T. Mauritsen, H. Tatebe, Enhanced warming constrained by past trends in equatorial Pacific sea surface temperature gradient. *Nat. Clim. Change* **11**, 33–37 (2021).
10. S. McGregor *et al.*, Recent Walker circulation strengthening and Pacific cooling amplified by Atlantic warming. *Nat. Clim. Change* **4**, 888–892 (2014).
11. G. Li, S.-P. Xie, Y. Du, Y. Luo, Effects of excessive equatorial cold tongue bias on the projections of tropical Pacific climate change. Part I: The warming pattern in CMIP5 multi-model ensemble. *Clim. Dyn.* **47**, 3817–3831 (2016).
12. G. A. Meehl, A. Hu, H. Teng, Initialized decadal prediction for transition to positive phase of the Interdecadal Pacific Oscillation. *Nat. Commun.* **7**, 11718 (2016).
13. S. Po-Chedley *et al.*, Natural variability contributes to model–satellite differences in tropical tropospheric warming. *Proc. Natl. Acad. Sci. U.S.A.* **118**, e2020962118 (2021).
14. S. Power *et al.*, Decadal climate variability in the tropical Pacific: Characteristics, causes, predictability, and prospects. *Science* **374**, eaay9165 (2021).
15. M. Newman *et al.*, The Pacific decadal oscillation. Revisited. *J. Clim.* **29**, 4399–4427 (2016).
16. T. R. Ault, C. Deser, M. Newman, J. Emile-Geay, Characterizing decadal to centennial variability in the equatorial Pacific during the last millennium. *Geophys. Res. Lett.* **40**, 3450–3456 (2013).
17. I. M. Held *et al.*, Probing the fast and slow components of global warming by returning abruptly to preindustrial forcing. *J. Clim.* **23**, 2418–2427 (2010).
18. S.-M. Long, S.-P. Xie, X.-T. Zheng, Q. Liu, Fast and slow responses to global warming: Sea surface temperature and precipitation patterns. *J. Clim.* **27**, 285–299 (2014).
19. U. K. Heede, A. V. Fedorov, N. J. Burls, A stronger versus weaker Walker: Understanding model differences in fast and slow tropical Pacific responses to global warming. *Clim. Dyn.* **57**, 2505–2522 (2021).
20. U. K. Heede, A. V. Fedorov, Colder eastern equatorial Pacific and stronger walker circulation in the early 21st century: Separating the forced response to global warming from natural variability. *Geophys. Res. Lett.* **50**, e2022GL101020 (2023).
21. A. C. Clement, R. Seager, M. A. Cane, S. E. Zebiak, An ocean dynamical thermostat. *J. Clim.* **9**, 2190–2196 (1996).
22. I. M. Held, B. J. Soden, Robust responses of the hydrological cycle to global warming. *J. Clim.* **19**, 5686–5699 (2006).
23. T. R. Knutson, S. Manabe, Time-mean response over the tropical pacific to increased CO2 in a coupled ocean-atmosphere model. *J. Clim.* **8**, 2181–2199 (1995).
24. S.-P. Xie *et al.*, Global warming pattern formation: Sea surface temperature and rainfall. *J. Clim.* **23**, 966–986 (2010).
25. R. Seager *et al.*, Strengthening tropical Pacific zonal sea surface temperature gradient consistent with rising greenhouse gases. *Nat. Clim. Change* **9**, 517–522 (2019).
26. C. Takahashi, M. Watanabe, Pacific trade winds accelerated by aerosol forcing over the past two decades. *Nat. Clim. Change* **6**, 768–772 (2016).
27. D. M. Smith *et al.*, Role of volcanic and anthropogenic aerosols in the recent global surface warming slowdown. *Nat. Clim. Change* **6**, 936–940 (2016).
28. U. K. Heede, A. V. Fedorov, Eastern equatorial Pacific warming delayed by aerosols and thermostat response to CO2 increase. *Nat. Clim. Change* **11**, 696–703 (2021).
29. C. Deser *et al.*, Isolating the evolving contributions of anthropogenic aerosols and greenhouse gases: A new CESM1 large ensemble community resource. *J. Clim.* **33**, 7835–7858 (2020).
30. S. M. Kang, S.-P. Xie, C. Deser, B. Xiang, Zonal mean and shift modes of historical climate response to evolving aerosol distribution. *Sci. Bull.* **66**, 2405–2411 (2021).
31. M. B. Menary *et al.*, Aerosol-forced AMOC changes in CMIP6 historical simulations. *Geophys. Res. Lett.* **47**, e2020GL088166 (2020).
32. B. B. B. Booth, N. J. Dunstone, P. R. Halloran, T. Andrews, N. Bellouin, Aerosols implicated as a prime driver of twentieth-century North Atlantic climate variability. *Nature* **484**, 228–232 (2012).
33. T. Verma, R. Saravanan, P. Chang, S. Mahajan, Tropical pacific ocean dynamical response to short-term sulfate aerosol forcing. *J. Clim.* **32**, 8205–8221 (2019).
34. B. L. Otto-Bliesner *et al.*, Climate variability and change since 850 CE: An ensemble approach with the community earth system model. *Bull Am. Meteorol. Soc.* **97**, 735–754 (2016).
35. H. Kim, S. M. Kang, J. E. Kay, S.-P. Xie, Subtropical clouds key to Southern Ocean teleconnections to the tropical Pacific. *Proc. Natl. Acad. Sci. U.S.A.* **119**, e2200514119 (2022).
36. Y. Y. Planton *et al.*, Evaluating climate models with the CLIVAR 2020 ENSO metrics package. *Bull Am. Meteorol. Soc.* **102**, E193–E217 (2021).
37. S. M. Kang, I. M. Held, D. M. W. Frierson, M. Zhao, The response of the ITCZ to extratropical thermal forcing: Idealized slab-ocean experiments with a GCM. *J. Clim.* **21**, 3521–3532 (2008).
38. T. Schneider, T. Bischoff, G. H. Haug, Migrations and dynamics of the intertropical convergence zone. *Nature* **513**, 45–53 (2014).
39. Y.-T. Hwang, D. M. W. Frierson, S. M. Kang, Anthropogenic sulfate aerosol and the southward shift of tropical precipitation in the late 20th century. *Geophys. Res. Lett.* **40**, 2845–2850 (2013).
40. S. Hu, A. V. Fedorov, Cross-equatorial winds control El Niño diversity and change. *Nat. Clim. Change* **8**, 798–802 (2018).
41. F. S. R. Pausata, D. Zanchettin, C. Karamperidou, R. Caballero, D. S. Battisti, ITCZ shift and extratropical teleconnections drive ENSO response to volcanic eruptions. *Sci. Adv.* **6**, eaaz5006 (2020).
42. M. E. Mann, M. A. Cane, S. E. Zebiak, A. Clement, Volcanic and solar forcing of the tropical pacific over the past 1000 years. *J. Clim.* **18**, 447–456 (2005).
43. H. Zhang, C. Deser, A. Clement, R. Tomas, Equatorial signatures of the pacific meridional modes: Dependence on mean climate state. *Geophys. Res. Lett.* **41**, 568–574 (2014).
44. Y.-T. Hwang, S.-P. Xie, C. Deser, S. M. Kang, Connecting tropical climate change with Southern Ocean heat uptake. *Geophys. Res. Lett.* **44**, 9449–9457 (2017).
45. S. M. Kang *et al.*, Walker circulation response to extratropical radiative forcing. *Sci. Adv.* **6**, eabd3021 (2020).
46. W.-T. Hsiao, Y.-T. Hwang, Y.-J. Chen, S. M. Kang, The role of clouds in shaping tropical pacific response pattern to extratropical thermal forcing. *Geophys. Res. Lett.* **49**, e2022GL098023 (2022).
47. H.-Y. Tseng *et al.*, Fast and slow responses of the tropical pacific to radiative forcing in northern high latitudes. *J. Clim.* **36**, 1–31 (2023).
48. S.-P. Xie *et al.*, Similar spatial patterns of climate responses to aerosol and greenhouse gas changes. *Nat. Geosci.* **6**, 828–832 (2013).
49. N. J. Burls, L. Muir, E. M. Vincent, A. Fedorov, Extra-tropical origin of equatorial Pacific cold bias in climate models with links to cloud albedo. *Clim. Dyn.* **49**, 2093–2113 (2017).
50. Z. Liu, B. Huang, A coupled theory of tropical climatology: Warm pool, cold tongue, and walker circulation. *J. Clim.* **10**, 1662–1679 (1997).
51. A. Capotondi, B. Qiu, Decadal variability of the pacific shallow overturning circulation and the role of local wind forcing. *J. Clim.* **36**, 1001–1015 (2023).
52. A. Capotondi, M. A. Alexander, C. Deser, M. J. McPhaden, Anatomy and decadal evolution of the pacific subtropical-tropical cells (STCs). *J. Clim.* **18**, 3739–3758 (2005).
53. M. T. Luongo, S.-P. Xie, I. Eisenman, Buoyancy forcing dominates the cross-equatorial ocean heat transport response to northern hemisphere extratropical cooling. *J. Clim.* **35**, 6671–6690 (2022).
54. M. J. McPhaden, D. Zhang, Pacific Ocean circulation rebounds. *Geophys. Res. Lett.* **31**, L18301 (2004).
55. J. E. Kay *et al.*, The community earth system model (CESM) large ensemble project: A community resource for studying climate change in the presence of internal climate variability. *Bull Am. Meteorol. Soc.* **96**, 1333–1349 (2015).
56. H.-Y. Tseng, Data for PNAS 2023. Figshare. https://doi.org/10.6084/m9.figshare.24581016. Deposited 17 November 2023.